ACS APPLIED MATERIALS & INTERFACES

www.acsami.org

Research Article

Preparation of Twisted Bilayer Graphene via the Wetting Transfer Method

Yuan Hou, Xibiao Ren, Jingcun Fan, Guorui Wang, Zhaohe Dai, Chuanhong Jin, Wenxiang Wang, Yinbo Zhu, Shuai Zhang, Luqi Liu,* and Zhong Zhang*

Cite This: *ACS Appl. Mater. Interfaces* 2020, 12, 40958–40967

Read Online

ACCESS | Metrics & More | Article Recommendations | Supporting Information

ABSTRACT: Assembling monolayers into a bilayer system unlocks the rotational free degree of van der Waals (vdW) homo/heterostructure, enabling the building of twisted bilayer graphene (tBLG) which possesses novel electronic, optical, and mechanical properties. Previous methods for preparation of homo/heterstructures inevitably leave the polymer residue or hexagonal boron nitride (*h*-BN) mask, which usually obstructs the measurement of intrinsic mechanical and surface properties of tBLG. Undoubtedly, to fabricate the designable tBLG with clean interface and surface is necessary but challenging. Here, we propose a simple and handy method to prepare atomically clean twisted bilayer graphene with controllable twist angles based on wetting-induced delamination. This method can transfer tBLG onto a patterned substrate, which offers an excellent platform for the observation of physical phenomena such as relaxation of moiré pattern in marginally tBLG. These findings and insight should ultimately guide the designable packaging and atomic characterization of the two-dimensional (2D) materials.

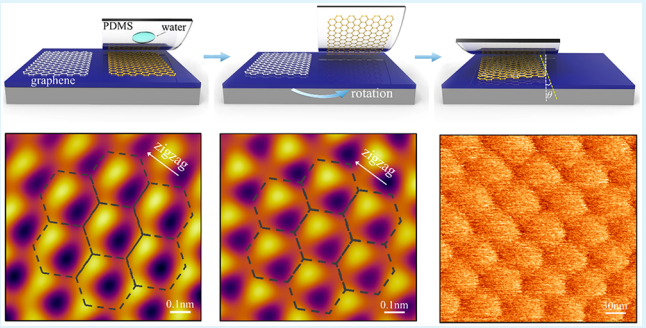

KEYWORDS: *twisted bilayer graphene, wet transfer, moiré pattern, interface, capillary force*

INTRODUCTION

Twisted bilayer graphene (tBLG), consisting of two atomically graphene monolayers with van der Waals (vdW) coupling,[1] has been the research hot spot due to its unique physical properties, such as the van Hove singularities,[2,3] superconductivity,[4,5] and superlubricity.[6] More interestingly, once graphene sheets are stacked at the marginally small angles (<1°, *m*-tBLG), the atomic reconstruction will lead to the formation of a unique moiré pattern with triangular boundaries.[7−9] Such a long-period moiré pattern with a network of domain walls (DWs) endows the graphene with fascinating solitonic properties (e.g., valley-polarized transport channels[10,11] and reflect plasmons[12]). To fully explore 2D material properties and fabricate 2D homo/heterostructures, a clean and intact transfer from the initial substrate onto target area without damaging their intrinsic physical properties and, in particular, without any chemical contamination is fundamentally essential.[13]

So far, several transfer methods have been developed to stack different 2D materials in vdW heterostructures, including the polymer-based sacrificial layer method,[14−17] the polydimethylsiloxane (PDMS)-based all-dry transfer method,[18] and the vdW pickup transfer method.[19,20] The most popular method for assembling 2D heterostructures is by using *h*-BN flakes as a "transfer tape", which arises from the strong vdW interaction between graphene and *h*-BN.[21−23] However, the presence of *h*-BN and polymer residues on the graphene surface would impact the structure characterization, intrinsic physical properties as well as the following device performance of tBLG.[24−26] Therefore, the fabrication of a tBLG sample with minimal masks (i.e., polymer residuals and *h*-BN) remains a challenge, achieving which would enable a number of previously elusive characterizations on the intrinsic structural properties of tBLG, for example, moiré patterns of tBLG.[27]

Recently, a capillary force stemming from liquid film has been used to transfer 2D materials and fabricate vdW heterostructures[15,28,29] or most recently for soft materials printing.[30,31] However, the critical problem in the capillary force dominated transfer process is that surface tension of water might damage the ultrathin flakes. For instance, once the water penetrated into the graphene/SiO_2 interface, the capillary force can cause the tensile stress and even fracture in graphene layer. Thus, two critical issues have to been considered: (i) the capillary force induced the damage of graphene; (ii) the polymer layer caused surface pollution.

Received: July 3, 2020
Accepted: August 11, 2020
Published: August 11, 2020

https://dx.doi.org/10.1021/acsami.0c12000
ACS Appl. Mater. Interfaces 2020, 12, 40958–40967

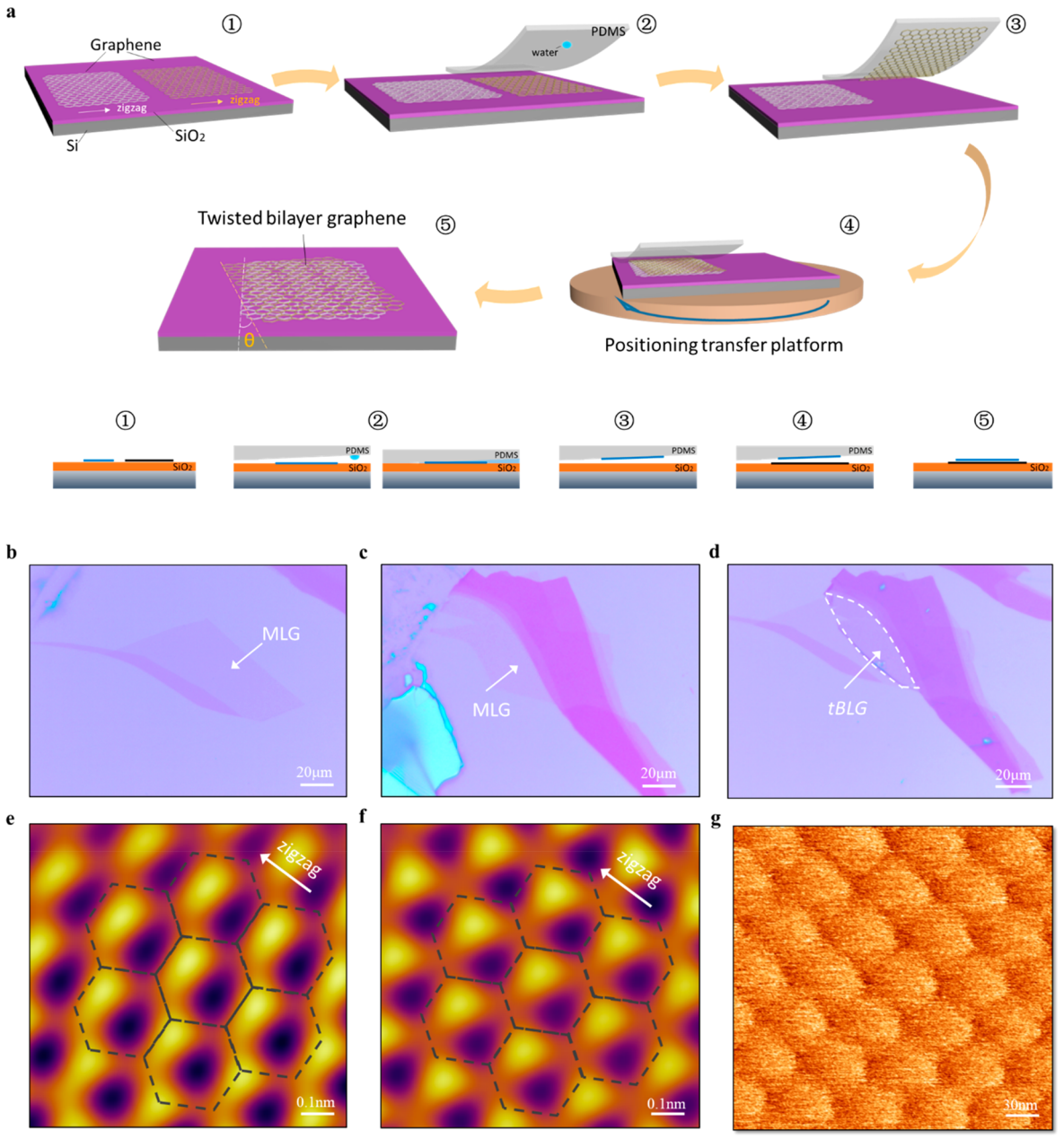

Figure 1. Fabrication of twisted bilayer graphene. (a) Schematic illustration of the wetting transfer process for tBLG. (b, c) Optical images of adjacent mechanical exfoliated monolayer graphenes (MLGs) on SiO_2/Si substrate. (d) Optical images of tBLG fabricated by graphene monolayers via the wetting transfer method. The dashed lines show the stacking region. (e, f) Images of lateral force signal of monolayer graphenes in (b) and (c), respectively, white arrows indicate the lattice orientations. (g) Lateral force images of freestanding *m*-tBLG showing the clear moiré pattern.

Motivated by these issues, in this work, we propose a wetting assisted transfer strategy for the direct transfer and deterministic assembly of graphene monolayers. Combining with MD simulation and theoretical analysis, we deduce an energy criterion for this wetting transfer process. In experiment, we employ a water droplet modified PDMS film as adhesive glue to grab monolayer graphene from the SiO_2 substrate.[29,30] Through modifying the hydrophilicity of SiO_2 substrate, we can successfully detach monolayer graphene from the SiO_2/Si substrate with indiscernible mechanical damage, followed by stacking two monolayer graphenes to form tBLG structure with controllable twist angles. On the basis of this method, we characterize a freestanding *m*-tBLG sample by micro-Raman spectroscopy and dark field transmission electron microscopy (DF-TEM) and further reveal the uniformity of twist angles of samples within the tested regions.

RESULTS AND DISCUSSION

Figure 1a illustrates the schematic drawing of the droplet-assistant transfer process for graphene monolayers. Through the mechanical exfoliation method,[32] several monolayer graphene sheets with ∼100 μm lateral size were directly deposited onto plasma-treated SiO_2/Si substrate. Then we can find several monolayer graphene sheets with the same crystal orientation. According to earlier works, a thin layer of liquid (e.g., water) has been successfully used as an instant glue to pick up 2D materials,[29] while the water-induced surface tension might fold and even damage 2D materials, making the

https://dx.doi.org/10.1021/acsami.0c12000
ACS Appl. Mater. Interfaces 2020, 12, 40958−40967

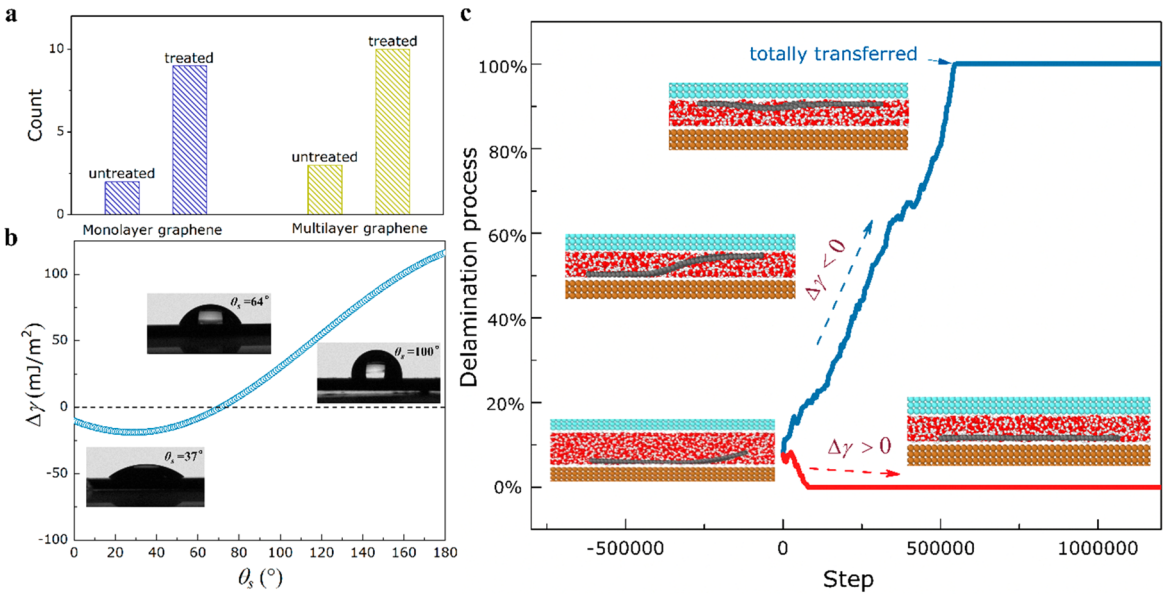

Figure 2. Wetting-induced delamination mechanism. (a) Comparison of the success rate of graphene transfer on untreated and treated substrates. (b) Change of energy differences with increasing contact angle θ_s. The region labeled by solid dashed line is the energy criteria for transferring monolayer graphene. (c) MD simulations showing the delamination process of graphene with different interactions between water and substrate. The insets indicate the snapshots of MD simulation results in transfer process. The stress distribution can be seen in Movies S3 and S4.

precise positioning more difficult. In our method, we attach a single water droplet to a wedge PDMS film (2 mm × 2 mm) in the view of optical microscope, and then we can easily move the droplet to the top of graphene/SiO_2 substrate. We carefully control the position between PDMS film and graphene/SiO_2/Si substrate to ensure water droplet entrapped within the graphene/SiO_2 interface to weaken the strong adhesion energy (100−400 mJ/m^2).[33,34] After lifting one of the monolayer graphene sheet, we can translate the PDMS/graphene to the top of the other graphene sheet. Finally, the graphene on PDMS can be attached to the other graphene through conventional PDMS transfer method.[18]

Note that the key step in the above transfer process is to detach monolayer graphene from the SiO_2/Si substrate without damage. Previous work often utilized the polymeric coating layers (e.g., poly(methyl methacrylate) or poly(propylene carbonate)) as prepared by spin-coating technology;[35] however, these protective layers were difficult to clean up. Herein, we focus on the optimization of transfer step and improvement of success rate of transfer. We conducted two ways to lift graphene in the transfer process: (1) water contacts with graphene first and (2) PDMS contacts with graphene first. In the first case, the water droplet first contacts the graphene as the PDMS closing to the substrate (Figure S1a,b). The water droplet might penetrate the interface between graphene and substrate due to the strong interaction between water and substrate. This means the graphene would be lifted first and then tend to float on the surface of droplet. In this step, the surface tension of water may cause the large tensile stress in the graphene layer due to the absence of the supporting layer. As the droplet spreads across the graphene layer, the entire graphene could be broken. In comparison, in the second case, most regions of the graphene sheets remain intact (Figure S1c,d). When the water spreads to break the interface between graphene and substrate, the lifted graphene will attach to the PDMS. Thanks to the van der Waals interaction between graphene and PDMS, the monolayer graphene could be lifted with minimal damage. In other words, PDMS can act as the support layer to minimize the tensile stress in the lifted graphene layer. On the basis of this observation, we designed a wedge-shaped PDMS film to ensure the graphene layers contacts PDMS first (Figure S2). Consequently, the monolayer graphene sheet could be easily peeled off from the substrate and then adhere onto the PDMS stamp (Figure S3). Meanwhile, the detached monolayer graphene sheet would keep the crystal orientation due to the supporting of PDMS film, which is beneficial for controlling the twist angle, as verified in Figure 1b−d.

To understand the underlying mechanism of such water droplet assisted delamination, we prepared four groups of samples including monolayer and multilayer graphene on the treated and untreated substrates. The detailed surface treatment process of substrate and measurement of contact angles are illustrated in Figure S4. There are ten samples in each group, and the statistical data of successful transferred samples are summarized in Figure 2a. The surface treatment of the substrate significantly affects the success rate of transfer for graphene flakes. Figure S5a−d shows that graphene flakes on the untreated substrate were difficult to be lifted. Comparatively, the graphene flakes on the treated substrate were easily transferred in Figure S5e−h. The whole transfer process can be seen in Movies S1 and S2.

According to the above experimental results, we infer that the hydrophilicity of the surface is more favorable to the transfer of graphene. To further study the mechanism of this phenomenon, we propose a simplified one-dimensional (1D) mechanical model. In this work, we show a wetting-induced delamination for this water-assistant transfer process. The success of such transfer is dependent on the energy difference between the initial and final configurations. Therefore, we can write the energy change per area ($\Delta\gamma$) as

$$\Delta\gamma = \gamma_{gp} - \gamma_{wp} + \gamma_{ws} - \gamma_{gs} \quad (1)$$

https://dx.doi.org/10.1021/acsami.0c12000
ACS Appl. Mater. Interfaces 2020, 12, 40958−40967

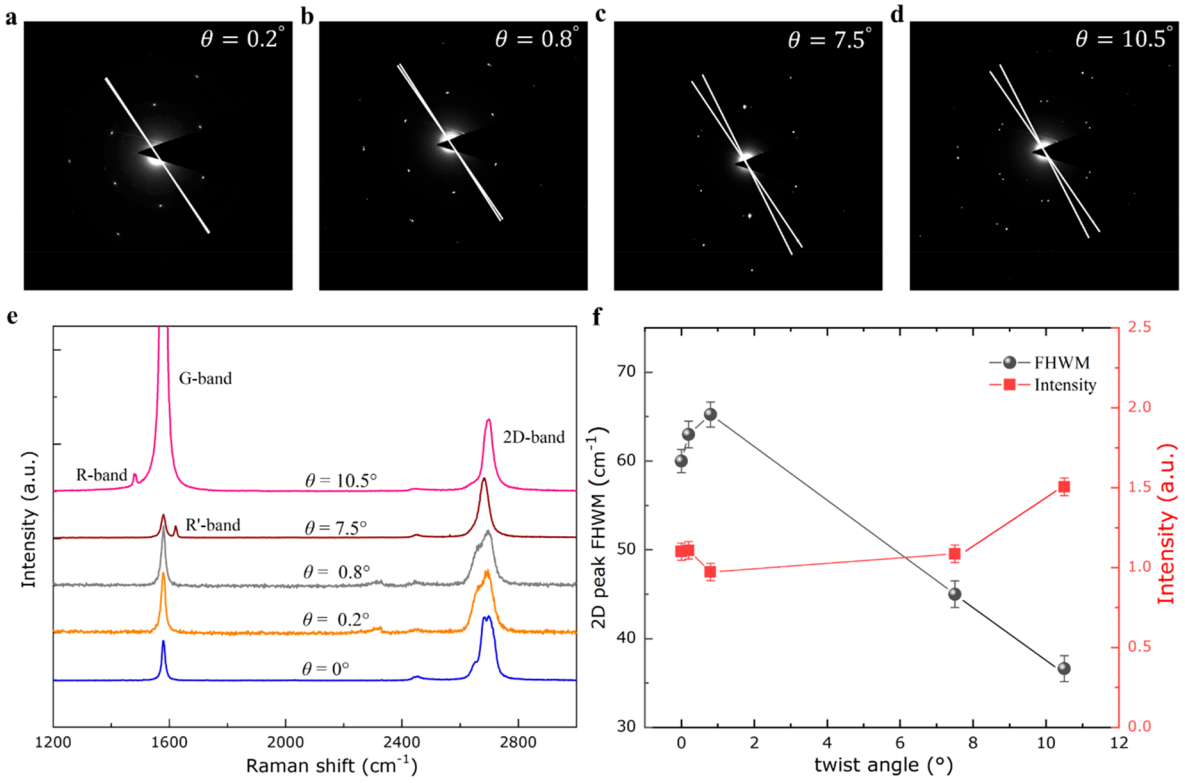

Figure 3. Characterization of twist angles. (a–d) SAED results of four typical tBLGs showing different twist angles. (e) Raman spectrum characterized based on samples in (a–d). (f) FHWM and intensity of 2D peaks of tBLGs with different twist angles.

where γ_{gp}, γ_{wp}, γ_{ws}, and γ_{gs} represent the interaction energy per area between graphene and PDMS, water and PDMS, water and substrate, and graphene and substrate, respectively. The spontaneous transfer would occur if the system energy is reduced, i.e., $\Delta\gamma < 0$, which implies

$$\gamma_{gp} - \gamma_{gs} < \gamma_p - \gamma_s + \gamma_w(\cos\theta_s - \cos\theta_p) \quad (2)$$

where we applied Young's equation; γ_w is the surface tension coefficient of water, γ_p is the surface energy of PDMS, γ_s is the surface energy of substrate, θ_s is the contact angle between substrate and water, and θ_p is the contact angle between PDMS and water. A more understandable form takes

$$\Gamma_{gs} - \Gamma_{gp} < \gamma_w(\cos\theta_s - \cos\theta_p) \quad (3)$$

where we applied the definition of adhesion, Γ_{gs} is the adhesion energy between graphene and SiO_2 substrate, and Γ_{gp} is the adhesion energy between graphene and PDMS. We find that the transfer would be energetically favored when the water-associated surface energies can make up the adhesion difference between graphene/SiO_2 and graphene/polymer. Immediately, the wetting transfer method can be optimized by using high-surface-energy liquid, superhydrophilic substrate, and superhydrophobic polymer film.

The contact angles θ_s and θ_p are related to the hydrophilicity of SiO_2 substrate and PDMS, respectively,[36,37] and are experimentally tuned, for instance, by O_2 plasma treatment of SiO_2 substrate. We select that Γ_{gs} and Γ_{gp} are 100 mJ/m^2 and 40 mJ/m^2, respectively, according to experimental measurements. Figure 2b shows the dependence of energy difference $\Delta\gamma$ on the contact angle θ_s where the contact angle θ_p is fixed to 120°.[37] In this case, the hydrophilic surface of the substrate would allow the transfer of the sheet (i.e., $\Delta\gamma < 0$) when $\theta_s < 70°$. In our experiments, θ_s is indeed 37°.

To further demonstrate the energy difference $\Delta\gamma$ determined wetting assisted delamination mechanism, we performed molecular dynamics (MD) simulations with different interaction between water and substrate. As shown in Figure 2c, monolayer graphene was first placed on the underlying substrate with a slightly prelifted edge where the gap was filled with water molecules. A gap of ~5 nm was set in the model, and the contact angles in the MD models are shown in Figure S6. Driven by the hydrophilic interaction between water and the underlying substrate, water molecules tend to spread forward on the SiO_2 substrate (termed as wetting).[36] As expected, when the water–substrate interaction is modified such that $\Delta\gamma = -20$ mJ/m^2, water molecules enter into the graphene–substrate interface (gap) spontaneously. As a result, the graphene monolayer is released by the substrate and adheres to the upper hydrophobic layer to decrease its contact with water molecules.

For the fabrication of tBLG, except for lifting monolayer graphene, another important step comes from the efficient design of twist angles. Note that by mechanical exfoliation we can easily obtain two adjacent monolayer graphene sheets with the same crystal orientation, which is convenient to control the rotational alignment of the layer-by-layer stacked graphene sheets. Figure 1b,c presents the optical images of the mechanically exfoliated individual graphene sheets deposited onto the SiO_2/Si substrate. Generally, the straight edges in mechanically exfoliated monolayer graphene sheets were selected as crystallographic references to determine the crystal orientation.[38] However, limited by the optical resolution, the straight edges are often a mixture of both zigzag and armchair segments instead of purely zigzag or armchair, which would

https://dx.doi.org/10.1021/acsami.0c12000
ACS Appl. Mater. Interfaces 2020, 12, 40958–40967

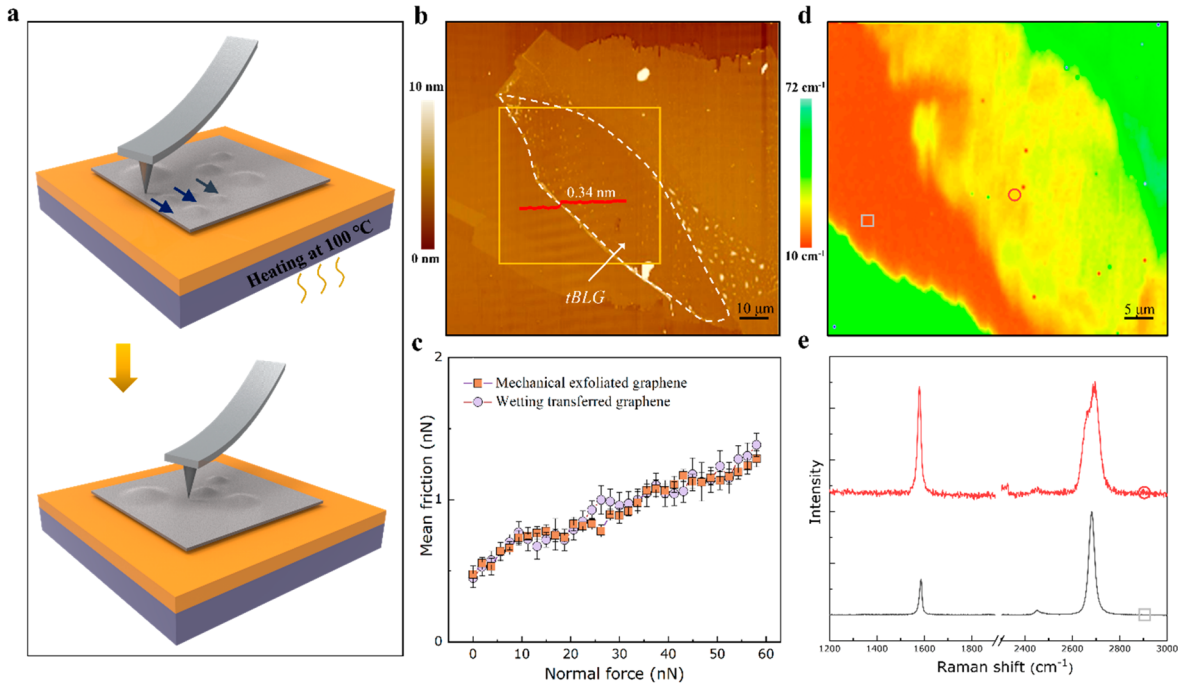

Figure 4. Characterization of the surface and interface of tBLG sample obtained by the wetting transfer method. (a) Schematic of mechanical and heating treatment. (b) AFM topology taken from the tBLG on SiO_2/Si substrate and the white dashed line indicating the tBLG region. (c) Friction forces measured on mechanical exfoliated and wetting transferred graphene. (d) Raman mapping image showing the FWHM of the 2D peak (2700 cm^{-1}) of the solid box labeled region in (b). (e) Typical Raman spectrum of different regions corresponding to the square and circle marks in (d).

challenge the accuracy of the crystal axes identification. Thus, we further employ a nondestructive and straightforward atomic force microscopy (AFM) method to determine the detailed zigzag or armchair crystal orientations.[39] The analysis based on fast Fourier transform (FFT) images reveals the lattice orientation of monolayer graphene sheet. We select two individual graphene sheets with the same crystal axes as components as presented in Figure 1e,f. Here, the controllable twist angle between two monolayer graphene sheets can be realized with the help of a rotation stage (the accuracy is ~0.2°). We advocate that the method presented in this work can be extended to build other 2D homostructures with long-period superlattices, such as the *m*-tBLG moiré pattern as shown in Figure 1g. Here, benefitting from the clean surface of such *m*-tBLG, we can obtain the clear image of such a long-period moiré pattern with a relaxed structure.

To demonstrate the relative twist angles of tBLGs samples fabricated by the wetting-assisted transfer method, we fabricated four samples with twist angles in a range of 0.2°–10.5° and characterized their twist angles by selected area electron diffraction (SAED). Figure 3a–d shows the SAED results of tBLG samples characterized by transmission electron microscopy (TEM), and the bright hexagonal diffraction spots reveal the crystal orientation of exfoliated graphene lattice. Note that most of tBLGs samples show two sets of hexagonal diffraction spots, which can be ascribed to the stacking of the two constituent monolayers. However, for the *m*-tBLG (θ < 1°), the twist angle is so small that the spacing between the two sets of spots is indistinguishable. Alternatively, in this case, the moiré pattern instead of hexagonal diffraction spots is used to identify the relative twist angles. As a case, Figure 1g presents the periodic moiré pattern of tBLGs with twist angle 0.2° characterized by lateral force microscopy.

To confirm the uniformity of the tBLGs fabricated by the wetting assisted transfer method, Raman spectra of the tBLGs samples are measured, with Bernal stacked bilayer graphene as reference. The same tBLGs samples are utilized for both Raman spectra and DF-TEM characterizations. As shown in Figure 3e, each Raman spectrum exhibits two distinct peaks at ~1580 cm^{-1}, corresponding to graphene G band, and at ~2700 cm^{-1}, corresponding to graphene 2D band.[40] For *m*-tBLG, similar to the Bernal stacked bilayer graphene, the 2D band is dispersive and can be fitted into four Lorentzian bands with slightly different frequencies compared to the monolayer graphene. While for tBLGs with relatively large twist angle, the R′ band originating from the graphene superlattice is activated at a low twist angle ($3° < \theta < 8°$), and the R′ frequency increases monotonically as the twist angle increases.[41] Besides, the large-twist-angle tBLG ($10° < \theta < 15°$) would exhibit ~20-fold of the enhanced Raman G band compared with the intensity of the 2D band.[41] Such an enhancement implies the strong interlayer interaction of π-bond electrons and the emergence of van Hove singularities (VHSs) with the appearance of R bands.[42] Because the 2D band is very sensitive to the electronic and phonon band structure of graphene,[40] we also further analyzed the full width at half-maximum (FWHM) and the intensity of the 2D peak with respect to the relative twist angles.[42] Figure 3f shows that with the increase of twist angles the FWHM of 2D peak increases slightly at small twist angle ($\theta < 1°$) but decreases significantly at larger twist angle ($\theta > 1°$). Meanwhile, the Raman 2D band intensity shows a contrary trend compared to that of the FWHM. Previous works have revealed that the Raman spectra of tBLGs strongly depend on the relative rotation angle between layers,[41,42] and the evolution of the Raman signature in our work agrees well with it, for example, the appearance of the R and R′ peaks.[41]

https://dx.doi.org/10.1021/acsami.0c12000
ACS Appl. Mater. Interfaces 2020, 12, 40958–40967

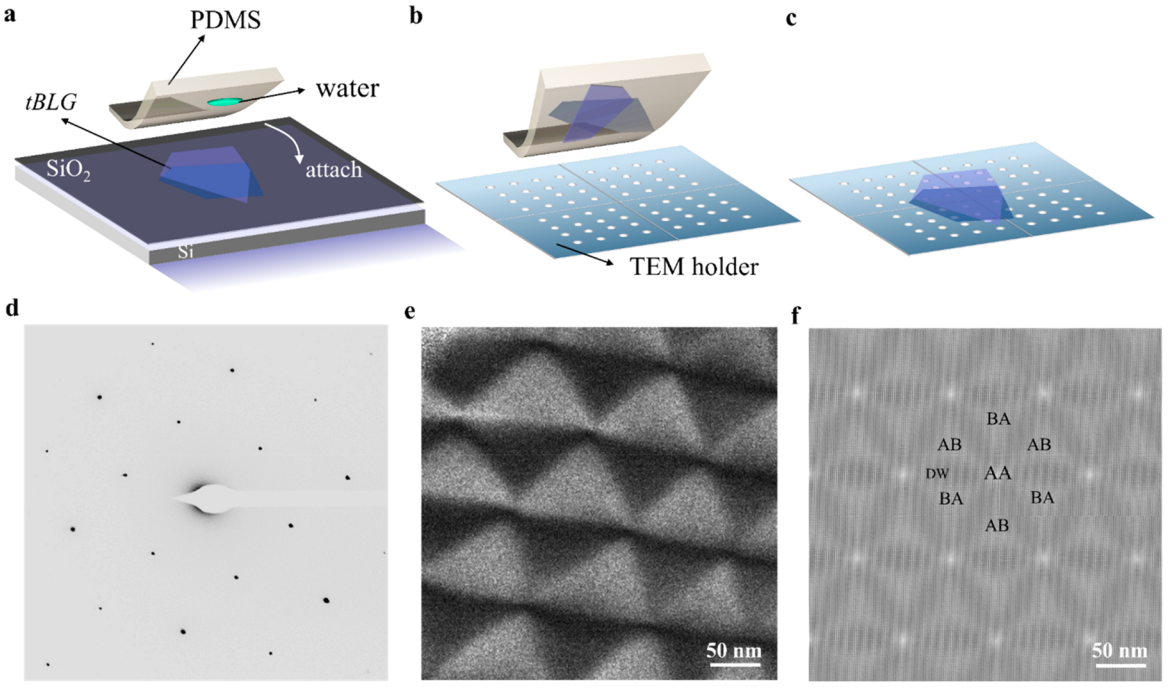

Figure 5. Freestanding *m*-tBLG characterized by HRTEM. (a–c) Schematic of the transfer process of freestanding tBLG. (d) Selected area electron diffraction (SAED) pattern of the *m*-tBLG from the freestanding area. (e) Dark-field image of the *m*-tBLG showing the long-period moiré pattern (93 nm, θ = 0.15°). (f) MD simulation of the relaxed moiré pattern indicating the AA, AB, DW, and BA stack regions.

Besides the designated twist angles in the fabrication of tBLG samples, the atomically clean interface is paramount to ensure intimate contact between the graphene flakes and fulfill their performance in electronic and optoelectronic devices.[43,44] However, contaminants such as water, hydrocarbon molecules, and ambient air are inevitably trapped between the interface.[13,33,45,46] The adhesive force at the interface often squeezes such contaminants into bubbles with size typically ranging from a few nanometers up to several micrometers.[33,47,48] To remove those contaminants, we applied the thermal and mechanical treatment sequence,[43,49] as illustrated in Figure 4a. We first heated the tBLG at ∼100 °C, which can make the bubbles physically mobile. Interestingly, heating treatment makes bubbles merge into larger size but does not remove the residues completely due to the lack of directional loading. To check the cleanness of the annealed sample, the lateral force was applied to the tBLG via the AFM tip scanning.[49] The AFM topography of the tBLG sample shown in Figure 4b indicates that most of interfacial contaminants have been removed after thermal and mechanical treatment. To demonstrate the intimate surface feature of tBLG on a SiO_2/Si substrate, we further conducted the friction tests by AFM. For comparison, the Bernal stacked bilayer graphene sample prepared by mechanical exfoliation method was used as a reference. Figure 4c shows the similar mean friction force versus normal force curves, implying the obtained clean surface of as-prepared tBLG sample. Furthermore, Figure 4e represents the typical Raman spectra of both the stacked and unstacked regions, corresponding to the twisted bilayer graphene and monolayer, respectively. The 2D band of the unstacked region can be fitted with a single Lorentzian peak (FWHM ∼24 cm^{-1} shown in Figure S7), as expected for monolayer graphene,[40] while the 2D band in the stacked region is achieved with four Lorentzian peaks. Specifically, for the *m*-tBLG sample, the FWHM of the 2D peak (∼65 cm^{-1}) is similar to that of AB stacked bilayer graphene.[40] The FWHM mapping of the 2D band in Figure 4d indicates that the FWHM in the stacked region is larger than that of the unstacked region, demonstrating high stack quality and uniformity of the tBLG samples. To thoroughly testify the quality of the transferred sample, we used conductive atomic force microscopy (c-AFM) to characterize the interfacial conductivity of twisted graphene layers (Figure S8), which reflects the interlayer coupling. The current signal exhibits the clear moiré pattern in the wrinkling–eliminating region. Considering the moiré pattern resulting from the interlayer vdW coupling, we believe that the twisted graphene layers possess the ultraclean interface and surface. In addition, we also prepared the typical FET (based on tBLG) by our transfer method, and the mobility of the carriers was estimated as be ∼2173 $cm^2\ V^{-1}\ s^{-1}$ (Figure S9), which is comparable to the values reported in the polymer-transferred AB-stacked bilayer graphene[50] and tBLG.[16]

A key advantage of our tBLG samples is that they can implement with suspended devices, without the limitation of *h*-BN which has been frequently used previously.[25] More interestingly, we can even achieve the recyclable transfer for the freestanding sample on patterned substrate, as shown in Figure S10. Through the repeated lift and drop steps (Figure 5a–c), we can further transfer the *m*-tBLG sample on the Si_3N_4 grid, as shown in the optical image in Figure S11. We employ dark-field transmission electron microscopy (DF-TEM) to explore its atomic structure of the *m*-tBLG sample. An aperture in the diffraction plane of the electron microscope selects electrons scattered through a narrow range of diffraction angles, distinguishing between regions of different crystallographic symmetries. The SAED pattern of the *m*-tBLG is shown in Figure 5d. The AB and BA stacking domains were imaged through the $[10\bar{1}0]$ diffraction angles as shown in Figure 5e. These shadow (AB) and light (BA) triangular

https://dx.doi.org/10.1021/acsami.0c12000
ACS Appl. Mater. Interfaces 2020, 12, 40958–40967

elements are densely laid to form hexagonal moiré pattern originating from marginally twist angle, also known as the relaxed moiré pattern.[7] Here, the period of moiré pattern (93 nm) represents that the twist angle is 0.15° according to the relationship between twist angle and moiré period.[51] The straight one-dimensional channels (DWs) formed along the boundary of triangular elements, which can exhibit extraordinary physical properties.[11,52] In addition, we found that the atomic dislocation in the DW region is perpendicular to the armchair direction, consistent with previous reports.[9] Here we also performed MD simulation using KC potential[53] as shown in Figure 5f, in which it can be concluded that the DW in the relaxed moiré pattern is shear solitons.[9] It is also worth mentioning that the freestanding *m*-tBLG fabricated by our method can be applied to achieve strain engineering to tune the moiré superlattice. For example, the moiré image in Figure 5e shows that the superlattice is easy to deform due to the presence of strain.[54]

CONCLUSION

In conclusion, using a facile wetting transfer method to delaminate monolayer graphene from the substrate, we achieve the supported and freestanding tBLG with a designable twist angle that offers a platform to explore the fancy properties of the moiré superlattice. On the basis of theoretical analysis and MD simulation results, we find that the successful transfer of graphene is mainly determined by the surface properties of the substrate and the transfer steps. This proposed mechanism can also be extended to the fabrication of other 2D material-based homo/heterostructure systems. Besides, the Raman, AFM, and TEM characterizations demonstrate the prepared tBLG possess the clean surface and interface. Finally, we succeed in fabricating the *m*-tBLG to study its relaxed moiré pattern.

METHODS

Sample Fabrication. The flake graphite from Shanghai Onway was used to mechanically exfoliate monolayer graphene sheet. The PDMS solution was made by using a mixture of Sylgard 184 prepolymer and curing agent with a 10:1 mol % ratio. After being dried in a vacuum dryer at 80−90 °C, the PDMS thin film (2 mm × 2 mm) was placed on the microtranslation stage which can be precisely controlled under optical microscopy. After dropping water on the PDMS surface, we quickly moved the stage to the top of graphene to avoid water evaporation. Then we kept the PDMS film gently close to the graphene surface. It should be noticed that the PDMS must contact graphene monolayers first to ensure the integrity of graphene. When the droplet on PDMS spread out the SiO_2 substrate, the PDMS stamp was quickly peeled off by lifting the stage. Next, the PDMS stamp with the lifted graphene monolayer was translated to the top of another marked monolayer graphene. Through rotating the underlying platform, we can set the rotation angle which can also be confirmed by optical micrographs. Thanks to a stronger vdW bonding between graphene interlayer, the graphene making contact with PDMS was easily attached to underlying graphene. Here, the twisted bilayer graphene was fabricated successfully since the PDMS detached from the substrate.

Characterization. The AFM (Asylum Research Cypher) was used to obtain atomic-resolution images and moiré pattern images. The AFM (Dimension Icon, Veeco) in the standard tapping mode was utilized to measure the topography of the tBLG, including the height profile. High-frequency Raman measurements were performed by using an Invo-Renishaw system with an incident wavelength of 514 nm. The spectral resolution was 1.0 cm^{-1}, and the spatial resolution was ~1 μm. The laser intensity was kept below 0.5 mW to avoid local heating induced by the laser. For the Raman scanning under various heights, Raman spectra from every spot of the sample were recorded with a step size of 100 nm. All featured bands in Raman spectra of graphene were fitted with Lorentzian functions to obtain the peak positions. Selected area electron diffraction (SAED) and HRTEM were done in a TEM (Titan G2 80-300, FEI) with a spherical aberration corrector on the imaging side and a monochromator that reduces the energy spread down to 0.15 eV. The microscope was operated at an acceleration voltage of 80 kV. In dark-field imaging, AB/BA domain contrast was obtained by taking the $g = 10\bar{1}0$ image with the specimen tilted of the zone axis (<5°). The electron diffraction patterns were acquired by a Gatan WA-Orius camera, and dark-field images and HRTEM images were obtained by a Gatan BM-UltraScan.

MD Simulations. The MD simulations in this work were performed by using a large-scale atomic/molecular massively parallel simulator (LAMMPS). A 5 × 5 nm^2 monolayer graphene sheet with a prelifted edge was placed on a solid substrate immersed in a 1.1 nm thick water film consisting of 4009 water molecules. The height of the prelifted edge was 4 Å, which is in correspondence with thermal fluctuation of graphene. Another solid platform was placed above the water as the substrate to be transferred onto. This initial configuration was built with the aid of the Packmol program.[55] Both the underlying and upper solid substrates were constructed based on the face-centered-cubic (FCC) lattice structure. A single point charge/extended (SPC/E) model was used to describe the water molecules.[56] The interactions among the carbon atoms in graphene sheet were described by the Tersoff potential.[57] The Lennard-Jones (LJ) potential was used to describe water−substrate and graphene−substrate interactions:

$$U_{LJ}(r) = 4\varepsilon\left[\left(\frac{\sigma}{r}\right)^{12} - \left(\frac{\sigma}{r}\right)^{6}\right]$$

where r is the distance between two atoms, ε is the strength of the interaction, and σ determines the distance at which the two atoms are at equilibrium. The cutoff length of all potentials was set to be r_c = 10 Å. The specific LJ parameters are listed in Table 1. The size of the simulation box is 122.4 × 122.4 × 34 $Å^3$. Periodic boundary conditions were applied in the x and y directions, and fix boundary conditions were used in the z direction. All the simulations were performed in the NVT ensemble with a time step of 1 fs. The temperature of graphene and water was kept constant at 298 K by employing a Nosé−Hoover thermostat.

Table 1. LJ Parameters for the MD Simulations

interaction pair	ε (eV)	σ (Å)
oxygen−oxygen	0.006734	3.166
carbon−oxygen	0.004020	3.283
carbon−lower substrate atom	0.006	3.0
carbon−upper substrate atom	0.001	3.0
oxygen−lower substrate atom	0.015, 0.025, 0.03	3.0
oxygen−upper substrate atom	0.0005	3.0
others	0.0	3.0

ASSOCIATED CONTENT

Supporting Information

The Supporting Information is available free of charge at https://pubs.acs.org/doi/10.1021/acsami.0c12000.

Materials and methods; Figures S1−S11 (PDF)

Movie S1 (AVI)

Movie S2 (AVI)

Movie S3 (AVI)

Movie S4 (AVI)

https://dx.doi.org/10.1021/acsami.0c12000
ACS Appl. Mater. Interfaces 2020, 12, 40958−40967

AUTHOR INFORMATION

Corresponding Authors

Luqi Liu − *CAS Key Laboratory of Nanosystem and Hierarchical Fabrication and CAS Center for Excellence in Nanoscience, National Center for Nanoscience and Technology, Beijing 100190, P. R. China;* orcid.org/0000-0002-5752-1638; Email: liulq@nanoctr.cn

Zhong Zhang − *CAS Key Laboratory of Mechanical Behavior and Design of Materials, Department of Modern Mechanics, University of Science and Technology of China, Hefei 230027, P. R. China; CAS Key Laboratory of Nanosystem and Hierarchical Fabrication and CAS Center for Excellence in Nanoscience, National Center for Nanoscience and Technology, Beijing 100190, P. R. China;* orcid.org/0000-0002-9102-1311; Email: zhong.zhang@nanoctr.cn

Authors

Yuan Hou − *CAS Key Laboratory of Mechanical Behavior and Design of Materials, Department of Modern Mechanics, University of Science and Technology of China, Hefei 230027, P. R. China; CAS Key Laboratory of Nanosystem and Hierarchical Fabrication and CAS Center for Excellence in Nanoscience, National Center for Nanoscience and Technology, Beijing 100190, P. R. China;* orcid.org/0000-0001-9307-5420

Xibiao Ren − *State Key Laboratory of Silicon Materials, School of Materials Science and Engineering, Zhejiang University, Hangzhou, Zhejiang 310027, P. R. China*

Jingcun Fan − *CAS Key Laboratory of Mechanical Behavior and Design of Materials, Department of Modern Mechanics, University of Science and Technology of China, Hefei 230027, P. R. China*

Guorui Wang − *CAS Key Laboratory of Nanosystem and Hierarchical Fabrication and CAS Center for Excellence in Nanoscience, National Center for Nanoscience and Technology, Beijing 100190, P. R. China*

Zhaohe Dai − *Department of Aerospace Engineering and Engineering Mechanics, The University of Texas at Austin, Austin, Texas 78712, United States;* orcid.org/0000-0002-5205-089X

Chuanhong Jin − *State Key Laboratory of Silicon Materials, School of Materials Science and Engineering, Zhejiang University, Hangzhou, Zhejiang 310027, P. R. China;* orcid.org/0000-0001-8845-5664

Wenxiang Wang − *CAS Key Laboratory of Nanosystem and Hierarchical Fabrication and CAS Center for Excellence in Nanoscience, National Center for Nanoscience and Technology, Beijing 100190, P. R. China*

Yinbo Zhu − *CAS Key Laboratory of Mechanical Behavior and Design of Materials, Department of Modern Mechanics, University of Science and Technology of China, Hefei 230027, P. R. China;* orcid.org/0000-0001-9204-9300

Shuai Zhang − *Applied Mechanics Laboratory, Department of Engineering Mechanics and Center for Nano and Micro Mechanics, Tsinghua University, Beijing 100084, P. R. China*

Complete contact information is available at: https://pubs.acs.org/10.1021/acsami.0c12000

Notes

The authors declare no competing financial interest.

ACKNOWLEDGMENTS

This work was jointly supported by National Natural Science Foundation of China (Grant Nos. 11890682, 11832010, 51772265, 51761165024, 61721005, and 21721002) and the Strategic Priority Research Program of Chinese Academy of Sciences (CAS) under Grant Nos. XDB30020100 and XDB36000000. X.R. and C.J. acknowledge financial support from the Zhejiang Provincial Natural Science Foundation under Grant No. D19E020002 and the 111 project under Grant No. B16042. The work on electron microscopy was done at the Center of Electron Microscopy of Zhejiang University. We are also grateful to Prof. Hengan Wu and Dr. Shizhe Feng for their help in our MD simulations as well as to Prof. Qunyang Li for his help in AFM characterization. We thank Prof. Bing Wang, Dr. Hai Hu, Mr. Yuantong Li and Dr. Jia Liu for their suggestions in our experiments.

REFERENCES

(1) Dos Santos, J. L.; Peres, N.; Neto, A. C. Graphene Bilayer with a Twist: Electronic Structure. *Phys. Rev. Lett.* **2007**, *99* (25), 256802.

(2) Liao, L.; Wang, H.; Peng, H.; Yin, J.; Koh, A. L.; Chen, Y.; Xie, Q.; Peng, H.; Liu, Z. Van Hove Singularity Enhanced Photochemical Reactivity of Twisted Bilayer Graphene. *Nano Lett.* **2015**, *15* (8), 5585−5589.

(3) Li, G. H.; Luican, A.; dos Santos, J. M. B. L.; Castro Neto, A. H.; Reina, A.; Kong, J.; Andrei, E. Y. Observation of Van Hove Singularities in Twisted Graphene Layers. *Nat. Phys.* **2010**, *6* (2), 109−113.

(4) Cao, Y.; Fatemi, V.; Demir, A.; Fang, S.; Tomarken, S. L.; Luo, J. Y.; Sanchez-Yamagishi, J. D.; Watanabe, K.; Taniguchi, T.; Kaxiras, E.; Ashoori, R. C.; Jarillo-Herrero, P. Correlated Insulator Behaviour at Half-Filling in Magic-Angle Graphene Superlattices. *Nature* **2018**, *556* (7699), 80−84.

(5) Cao, Y.; Fatemi, V.; Fang, S.; Watanabe, K.; Taniguchi, T.; Kaxiras, E.; Jarillo-Herrero, P. Unconventional Superconductivity in Magic-Angle Graphene Superlattices. *Nature* **2018**, *556* (7699), 43−50.

(6) Hod, O.; Meyer, E.; Zheng, Q.; Urbakh, M. Structural Superlubricity and Ultralow Friction across the Length Scales. *Nature* **2018**, *563* (7732), 485−492.

(7) Yoo, H.; Engelke, R.; Carr, S.; Fang, S.; Zhang, K.; Cazeaux, P.; Sung, S. H.; Hovden, R.; Tsen, A. W.; Taniguchi, T.; Watanabe, K.; Yi, G. C.; Kim, M.; Luskin, M.; Tadmor, E. B.; Kaxiras, E.; Kim, P. Atomic and Electronic Reconstruction at the Van Der Waals Interface in Twisted Bilayer Graphene. *Nat. Mater.* **2019**, *18* (5), 448−453.

(8) Butz, B.; Dolle, C.; Niekiel, F.; Weber, K.; Waldmann, D.; Weber, H. B.; Meyer, B.; Spiecker, E. Dislocations in Bilayer Graphene. *Nature* **2014**, *505* (7484), 533−537.

(9) Alden, J. S.; Tsen, A. W.; Huang, P. Y.; Hovden, R.; Brown, L.; Park, J.; Muller, D. A.; McEuen, P. L. Strain Solitons and Topological Defects in Bilayer Graphene. *Proc. Natl. Acad. Sci. U. S. A.* **2013**, *110* (28), 11256−11260.

(10) Rickhaus, P.; Wallbank, J.; Slizovskiy, S.; Pisoni, R.; Overweg, H.; Lee, Y.; Eich, M.; Liu, M.-H.; Watanabe, K.; Taniguchi, T.; Ihn, T.; Ensslin, K. Transport through a Network of Topological Channels in Twisted Bilayer Graphene. *Nano Lett.* **2018**, *18* (11), 6725−6730.

(11) Huang, S.; Kim, K.; Efimkin, D. K.; Lovorn, T.; Taniguchi, T.; Watanabe, K.; MacDonald, A. H.; Tutuc, E.; LeRoy, B. J. Topologically Protected Helical States in Minimally Twisted Bilayer Graphene. *Phys. Rev. Lett.* **2018**, *121* (3), No. 037702.

(12) Sunku, S. S.; Ni, G. X.; Jiang, B. Y.; Yoo, H.; Sternbach, A.; McLeod, A. S.; Stauber, T.; Xiong, L.; Taniguchi, T.; Watanabe, K.; Kim, P.; Fogler, M. M.; Basov, D. N. Photonic Crystals for Nano-Light in moiré Graphene Superlattices. *Science* **2018**, *362* (6419), 1153−1156.

(13) Haigh, S. J.; Gholinia, A.; Jalil, R.; Romani, S.; Britnell, L.; Elias, D. C.; Novoselov, K. S.; Ponomarenko, L. A.; Geim, A. K.;

Gorbachev, R. Cross-Sectional Imaging of Individual Layers and Buried Interfaces of Graphene-Based Heterostructures and Superlattices. *Nat. Mater.* **2012**, *11* (9), 764−767.
(14) Tan, Z.; Yin, J.; Chen, C.; Wang, H.; Lin, L.; Sun, L.; Wu, J.; Sun, X.; Yang, H.; Chen, Y.; Peng, H.; Liu, Z. Building Large-Domain Twisted Bilayer Graphene with Van Hove Singularity. *ACS Nano* **2016**, *10* (7), 6725−6730.
(15) Frisenda, R.; Navarro-Moratalla, E.; Gant, P.; Perez De Lara, D.; Jarillo-Herrero, P.; Gorbachev, R. V.; Castellanos-Gomez, A. Recent Progress in the Assembly of Nanodevices and Van Der Waals Heterostructures by Deterministic Placement of 2d Materials. *Chem. Soc. Rev.* **2018**, *47* (1), 53−68.
(16) Wang, B.; Huang, M.; Kim, N. Y.; Cunning, B. V.; Huang, Y.; Qu, D.; Chen, X.; Jin, S.; Biswal, M.; Zhang, X.; Lee, S. H.; Lim, H.; Yoo, W. J.; Lee, Z.; Ruoff, R. S. Controlled Folding of Single Crystal Graphene. *Nano Lett.* **2017**, *17* (3), 1467−1473.
(17) Chen, X. D.; Xin, W.; Jiang, W. S.; Liu, Z. B.; Chen, Y.; Tian, J. G. High-Precision Twist-Controlled Bilayer and Trilayer Graphene. *Adv. Mater.* **2016**, *28* (13), 2563−2570.
(18) Castellanos-Gomez, A.; Buscema, M.; Molenaar, R.; Singh, V.; Janssen, L.; van der Zant, H. S. J.; Steele, G. A. Deterministic Transfer of Two-Dimensional Materials by All-Dry Viscoelastic Stamping. *2D Mater.* **2014**, *1* (1), No. 011002.
(19) Wang, L.; Meric, I.; Huang, P. Y.; Gao, Q.; Gao, Y.; Tran, H.; Taniguchi, T.; Watanabe, K.; Campos, L. M.; Muller, D. A.; Guo, J.; Kim, P.; Hone, J.; Shepard, K. L.; Dean, C. R. One-Dimensional Electrical Contact to a Two-Dimensional Material. *Science* **2013**, *342* (6158), 614−617.
(20) Pizzocchero, F.; Gammelgaard, L.; Jessen, B. S.; Caridad, J. M.; Wang, L.; Hone, J.; Boggild, P.; Booth, T. J. The Hot Pick-up Technique for Batch Assembly of Van Der Waals Heterostructures. *Nat. Commun.* **2016**, *7*, 11894.
(21) Kim, K.; Yankowitz, M.; Fallahazad, B.; Kang, S.; Movva, H. C.; Huang, S.; Larentis, S.; Corbet, C. M.; Taniguchi, T.; Watanabe, K.; Banerjee, S. K.; LeRoy, B. J.; Tutuc, E. Van Der Waals Heterostructures with High Accuracy Rotational Alignment. *Nano Lett.* **2016**, *16* (3), 1989−1995.
(22) Yankowitz, M.; Ma, Q.; Jarillo-Herrero, P.; LeRoy, B. J. Van Der Waals Heterostructures Combining Graphene and Hexagonal Boron Nitride. *Nat. Rev. Phys.* **2019**, *1* (2), 112−125.
(23) Kim, K.; DaSilva, A.; Huang, S.; Fallahazad, B.; Larentis, S.; Taniguchi, T.; Watanabe, K.; LeRoy, B. J.; MacDonald, A. H.; Tutuc, E. Tunable moiré Bands and Strong Correlations in Small-Twist-Angle Bilayer Graphene. *Proc. Natl. Acad. Sci. U. S. A.* **2017**, *114*, 3364.
(24) Lin, Y.-C.; Lu, C.-C.; Yeh, C.-H.; Jin, C.; Suenaga, K.; Chiu, P.-W. Graphene Annealing: How Clean Can It Be? *Nano Lett.* **2012**, *12* (1), 414−419.
(25) Argentero, G.; Mittelberger, A.; Reza Ahmadpour Monazam, M.; Cao, Y.; Pennycook, T. J.; Mangler, C.; Kramberger, C.; Kotakoski, J.; Geim, A. K.; Meyer, J. C. Unraveling the 3d Atomic Structure of a Suspended Graphene/Hbn Van Der Waals Heterostructure. *Nano Lett.* **2017**, *17* (3), 1409−1416.
(26) Finney, N. R.; Yankowitz, M.; Muraleetharan, L.; Watanabe, K.; Taniguchi, T.; Dean, C. R.; Hone, J. Tunable Crystal Symmetry in Graphene−Boron Nitride Heterostructures with Coexisting moiré Superlattices. *Nat. Nanotechnol.* **2019**, *14* (11), 1029−1034.
(27) Chen, P.-Y.; Zhang, X.-Q.; Lai, Y.-Y.; Lin, E.-C.; Chen, C.-A.; Guan, S.-Y.; Chen, J.-J.; Yang, Z.-H.; Tseng, Y.-W.; Gwo, S.; Chang, C.-S.; Chen, L.-J.; Lee, Y.-H. Tunable moiré Superlattice of Artificially Twisted Monolayers. *Adv. Mater.* **2019**, *31*, 1901077.
(28) Zhang, Y.; Liu, Q. C.; Xu, B. X. Liquid-Assisted, Etching-Free, Mechanical Peeling of 2d Materials. *Extreme Mech. Lett.* **2017**, *16*, 33−40.
(29) Ma, X.; Liu, Q.; Xu, D.; Zhu, Y.; Kim, S.; Cui, Y.; Zhong, L.; Liu, M. Capillary-Force-Assisted Clean-Stamp Transfer of Two-Dimensional Materials. *Nano Lett.* **2017**, *17* (11), 6961−6967.
(30) Aghajamali, M.; Cheong, I. T.; Veinot, J. G. C. Water-Assisted Transfer Patterning of Nanomaterials. *Langmuir* **2018**, *34* (32), 9418−9423.
(31) Zhang, Y.; Yin, M.; Baek, Y.; Lee, K.; Zangari, G.; Cai, L.; Xu, B. Capillary Transfer of Soft Films. *Proc. Natl. Acad. Sci. U. S. A.* **2020**, *117* (10), 5210−5216.
(32) Huang, Y.; Sutter, E.; Shi, N. N.; Zheng, J.; Yang, T.; Englund, D.; Gao, H. J.; Sutter, P. Reliable Exfoliation of Large-Area High-Quality Flakes of Graphene and Other Two-Dimensional Materials. *ACS Nano* **2015**, *9* (11), 10612−10620.
(33) Sanchez, D. A.; Dai, Z.; Wang, P.; Cantu-Chavez, A.; Brennan, C. J.; Huang, R.; Lu, N. Mechanics of Spontaneously Formed Nanoblisters Trapped by Transferred 2d Crystals. *Proc. Natl. Acad. Sci. U. S. A.* **2018**, *115* (31), 7884−7889.
(34) Koenig, S. P.; Boddeti, N. G.; Dunn, M. L.; Bunch, J. S. Ultrastrong Adhesion of Graphene Membranes. *Nat. Nanotechnol.* **2011**, *6* (9), 543−546.
(35) Li, H.; Wu, J.; Huang, X.; Yin, Z.; Liu, J.; Zhang, H. A Universal, Rapid Method for Clean Transfer of Nanostructures onto Various Substrates. *ACS Nano* **2014**, *8* (7), 6563−6570.
(36) Satriano, C.; Marletta, G.; Kasemo, B. Oxygen Plasma-Induced Conversion of Polysiloxane into Hydrophilic and Smooth Siox Surfaces. *Surf. Interface Anal.* **2008**, *40* (3−4), 649−656.
(37) Bodas, D.; Khan-Malek, C. Hydrophilization and Hydrophobic Recovery of PDMS by Oxygen Plasma and Chemical Treatment—an SEM Investigation. *Sens. Actuators, B* **2007**, *123* (1), 368−373.
(38) You, Y.; Ni, Z.; Yu, T.; Shen, Z. Edge Chirality Determination of Graphene by Raman Spectroscopy. *Appl. Phys. Lett.* **2008**, *93* (16), 163112.
(39) Almeida, C. M.; Carozo, V.; Prioli, R.; Achete, C. A. Identification of Graphene Crystallographic Orientation by Atomic Force Microscopy. *J. Appl. Phys.* **2011**, *110* (8), No. 086101.
(40) Ferrari, A. C.; Meyer, J. C.; Scardaci, V.; Casiraghi, C.; Lazzeri, M.; Mauri, F.; Piscanec, S.; Jiang, D.; Novoselov, K. S.; Roth, S.; Geim, A. K. Raman Spectrum of Graphene and Graphene Layers. *Phys. Rev. Lett.* **2006**, *97* (18), 187401.
(41) Carozo, V.; Almeida, C. M.; Ferreira, E. H.; Cancado, L. G.; Achete, C. A.; Jorio, A. Raman Signature of Graphene Superlattices. *Nano Lett.* **2011**, *11* (11), 4527−4534.
(42) Kim, K.; Coh, S.; Tan, L. Z.; Regan, W.; Yuk, J. M.; Chatterjee, E.; Crommie, M.; Cohen, M. L.; Louie, S. G.; Zettl, A. Raman Spectroscopy Study of Rotated Double-Layer Graphene: Misorientation-Angle Dependence of Electronic Structure. *Phys. Rev. Lett.* **2012**, *108* (24), 246103.
(43) Purdie, D. G.; Pugno, N. M.; Taniguchi, T.; Watanabe, K.; Ferrari, A. C.; Lombardo, A. Cleaning Interfaces in Layered Materials Heterostructures. *Nat. Commun.* **2018**, *9* (1), 5387.
(44) Dean, C. R.; Young, A. F.; Meric, I.; Lee, C.; Wang, L.; Sorgenfrei, S.; Watanabe, K.; Taniguchi, T.; Kim, P.; Shepard, K. L.; Hone, J. Boron Nitride Substrates for High-Quality Graphene Electronics. *Nat. Nanotechnol.* **2010**, *5* (10), 722−726.
(45) Vasu, K. S.; Prestat, E.; Abraham, J.; Dix, J.; Kashtiban, R. J.; Beheshtian, J.; Sloan, J.; Carbone, P.; Neek-Amal, M.; Haigh, S. J.; Geim, A. K.; Nair, R. R. Van Der Waals Pressure and Its Effect on Trapped Interlayer Molecules. *Nat. Commun.* **2016**, *7*, 12168.
(46) Dai, Z.; Hou, Y.; Sanchez, D. A.; Wang, G.; Brennan, C. J.; Zhang, Z.; Liu, L.; Lu, N. Interface-Governed Deformation of Nanobubbles and Nanotents Formed by Two-Dimensional Materials. *Phys. Rev. Lett.* **2018**, *121* (26), 266101.
(47) Dai, Z.; Liu, L.; Zhang, Z. J. A. M. Strain Engineering of 2d Materials: Issues and Opportunities at the Interface. *Adv. Mater.* **2019**, *31*, 1805417.
(48) Khestanova, E.; Guinea, F.; Fumagalli, L.; Geim, A. K.; Grigorieva, I. V. Universal Shape and Pressure inside Bubbles Appearing in Van Der Waals Heterostructures. *Nat. Commun.* **2016**, *7*, 12587.
(49) Rosenberger, M. R.; Chuang, H. J.; McCreary, K. M.; Hanbicki, A. T.; Sivaram, S. V.; Jonker, B. T. Nano-"Squeegee" for the Creation

https://dx.doi.org/10.1021/acsami.0c12000
ACS Appl. Mater. Interfaces 2020, 12, 40958−40967

of Clean 2d Material Interfaces. *ACS Appl. Mater. Interfaces* **2018**, *10* (12), 10379−10387.
(50) Nguyen, V. L.; Perello, D. J.; Lee, S.; Nai, C. T.; Shin, B. G.; Kim, J.-G.; Park, H. Y.; Jeong, H. Y.; Zhao, J.; Vu, Q. A.; Lee, S. H.; Loh, K. P.; Jeong, S.-Y.; Lee, Y. H. Wafer-Scale Single-Crystalline Ab-Stacked Bilayer Graphene. *Adv. Mater.* **2016**, *28* (37), 8177−8183.
(51) Kuwabara, M.; Clarke, D. R.; Smith, D. A. Anomalous Superperiodicity in Scanning Tunneling Microscope Images of Graphite. *Appl. Phys. Lett.* **1990**, *56* (24), 2396−2398.
(52) Xu, S. G.; Berdyugin, A. I.; Kumaravadivel, P.; Guinea, F.; Krishna Kumar, R.; Bandurin, D. A.; Morozov, S. V.; Kuang, W.; Tsim, B.; Liu, S.; Edgar, J. H.; Grigorieva, I. V.; Fal'ko, V. I.; Kim, M.; Geim, A. K. Giant Oscillations in a Triangular Network of One-Dimensional States in Marginally Twisted Graphene. *Nat. Commun.* **2019**, *10* (1), 4008.
(53) Kolmogorov, A. N.; Crespi, V. H. Registry-Dependent Interlayer Potential for Graphitic Systems. *Phys. Rev. B: Condens. Matter Mater. Phys.* **2005**, *71* (23), 235415.
(54) Kerelsky, A.; McGilly, L. J.; Kennes, D. M.; Xian, L.; Yankowitz, M.; Chen, S.; Watanabe, K.; Taniguchi, T.; Hone, J.; Dean, C.; Rubio, A.; Pasupathy, A. N. Maximized Electron Interactions at the Magic Angle in Twisted Bilayer Graphene. *Nature* **2019**, *572* (7767), 95−100.
(55) Martínez, L.; Andrade, R.; Birgin, E. G.; Martínez, J. M. Packmol: A Package for Building Initial Configurations for Molecular Dynamics Simulations. *J. Comput. Chem.* **2009**, *30* (13), 2157−2164.
(56) Mark, P.; Nilsson, L. Structure and Dynamics of the Tip3p, Spc, and Spc/E Water Models at 298 K. *J. Phys. Chem. A* **2001**, *105* (43), 9954−9960.
(57) Lindsay, L.; Broido, D. Optimized Tersoff and Brenner Empirical Potential Parameters for Lattice Dynamics and Phonon Thermal Transport in Carbon Nanotubes and Graphene. *Phys. Rev. B: Condens. Matter Mater. Phys.* **2010**, *81* (20), 205441.

https://dx.doi.org/10.1021/acsami.0c12000
ACS Appl. Mater. Interfaces 2020, 12, 40958−40967